A Novel Approach to Experimental Studies of Mineral Dissolution Kinetics

Annual Technical Progress Report

Performance Period **September 1, 2004 – August 31, 2005**

CHEN ZHU
Indiana University

WILLIAM E. SEYFRIED
University of Minnesota

January 2005

Award Number **DE-FG26-04NT42125**

Department of Geological Sciences, Indiana University, Bloomington, IN 47401. Phone: (812) 855-5582, FAX: (812) 855-7899,
e-mail: czhu@indiana.edu

Disclaimer

Abstract

Currently, DOE is conducting pilot CO_2 injection tests to evaluate the concept of geological sequestration. One strategy that potentially enhances CO_2 solubility and reduces the risk of CO_2 leak back to the surface is dissolution of indigenous minerals in the geological formation and precipitation of secondary carbonate phases, which increases the brine pH and immobilizes CO_2. Clearly, the rates at which these dissolution and precipitation reactions occur directly determine the efficiency of this strategy. However, one of the fundamental problems in modern geochemistry is the persistent two to five orders of magnitude discrepancy between laboratory-measured and field derived feldspar dissolution rates. To date, there is no real guidance as to how to predict silicate reaction rates for use in quantitative models. Current models for assessment of geological carbon sequestration have generally opted to use laboratory rates, in spite of the dearth of such data for compositionally complex systems, and the persistent disconnect between lab and field applications. Therefore, a firm scientific basis for predicting silicate reaction kinetics in CO_2 injected geological formations is urgently needed to assure the reliability of the geochemical models used for the assessments of carbon sequestration strategies.
The funded experimental and theoretical study attempts to resolve this outstanding scientific issue by novel experimental design and theoretical interpretation to measure silicate dissolution rates and iron carbonate precipitation rates at conditions pertinent to geological carbon sequestration.

In the first year of the project, we have successfully developed a sample preparation method and completed three batch feldspar dissolution experiments at 200 ^{o}C and 300 bars. The changes of solution chemistry as dissolution experiments progressed were monitored with on-line sampling of the aqueous phase at the constant temperature and pressure. These data allow calculating overall apparent feldspar dissolution rates and secondary mineral precipitation rates as a function of saturation states. State-of-the-art atomic resolution transmission electron microscopy (TEM), scanning electron microscopy, and electron microprobe was used to characterize the reactants (feldspars before experiments). We experimented with different sample preparation methods for TEM study, and found excellent images and chemical resolution with reactants, which shows promise of the technology and establishes the baseline for comparison with products (feldspars after the experiments). Preliminary electron microscopic characterization shows that the reacted feldspars have etch pits and are covered with secondary sheet silicate phases. Reaction-path geochemical modeling is used to interpret the experimental results. We have established the software and database, and are making great progress.

Also during the first year, our education goal of graduate student training has been achieved. A Ph. D. student at Indiana University is progressing well in the degree program and has taken geochemical modeling, SEM, and TEM courses, which will facilitate research in the second and third year. A Ph. D. student at University of Minnesota is progressing well in conducting the experiments, and is near graduation. With the success of training of graduate students and excellent experimental data in the first year, we anticipate a more fruitful year in the second year.

Table of Contents

List of Figures and Tables

1. Introduction

There has been a great deal of concern over global climate change, and its link to growing atmospheric concentrations of carbon dioxide (CO_2). An ever-increasing amount of scientific evidence suggests that anthropogenic release of CO_2 has led to a rise in global temperatures over the past several hundred years (Crowley, 2000; Bradley, 2001). This "global warming" is a trend that, if unabated, can lead to significant and possibly catastrophic alteration of climate throughout the world.

In order to decrease the impact of CO_2 on global climate, several strategies are under development that will potentially remove CO_2 from the atmosphere or decrease CO_2 emission (Herzog et al., 1997; DOE, 1999). One such strategy that has received a great deal of attention involves the capture of CO_2 from large point sources (such as fossil fuel-fired power plants) and the long-term storage of CO_2 underground. In fact, such a technique is currently in practice in Norway. Statoil's Sleipner plant separates about 2,800 tons of CO_2 from a natural gas stream daily and injects it into a saline aquifer below the North Sea (Hammerstad, 2000).

For geological carbon sequestration programs that injects CO_2 into deep saline formations, the injected CO_2 can react with brine and solid matrix, resulting in an increase of pH and precipitation of carbonates. The rate of this reaction with respect to fluid flow is important to determine the mechanism of trapping, either by hydrodynamics (CO_2 dissolved in slow moving brine or remains to be in a separate liquid phase) or mineral trapping (carbon precipitation). Such processes are currently being evaluated at NETL sponsored pilot test sites in the Frio sandstone in the Texas Gulf Coast (Hovorka et al., 2002), at Statoil's Sliepner project in North Sea (Johnson et al., 2002), and at the Weyburn CO_2-enhanced oil recovery site, Canada (Perkins et al., 2002).

Recently, STRAZISAR et al. (2003) performed one-dimensional transport modeling of CO_2 in the Alberta basin, with the chemical reaction aspect of the model resembling that presented by GUNTER et al. (2000) as a first approximation. The ultimate goal of this modeling effort is to develop reservoir or basin scale models that include flow, mass and heat transport, multi-phases, and chemical reaction processes at field pilot test and CO_2 injection sites. Such a model is valuable for evaluating the suitability of a geological formation as CO_2 storage, optimal injection operations, and monitoring and management of injection operations.

One outcome of this modeling study is the demonstrated importance of mineral reaction kinetics. However, one of the fundamental problems in modern geochemistry is the persistent two to five orders of magnitude discrepancy between laboratory-measured and field derived feldspar dissolution rates (see reviews by Blum and Stillings, 1995; Drever and Clow, 1995; White, 1995). This discrepancy is huge. For example, the laboratory rates indicate that a 0.1 mm feldspar sphere should weather away in ~250 years, whereas the field rates predict a feldspar lifetime of millions of years (calculations followed Lasaga, 1998). Such a large discrepancy illustrates our inability to move forward with the quantitative assessment of mineral trapping as a sequestration strategy. In addition to the geological carbon sequestration program, kinetically controlled reactions, including glauconite dissolution (Gunter et al., 1997), iron carbonate precipitation (NRC, 2003), and olive and serpentine carbonation (Carey et al., 2003, and reports published by the Albany Research Center), are also important to other carbon sequestration programs.

To date, there is no real guidance as to how to predict *in situ* reaction rates for use in reactive transport models. Models for geological carbon sequestration have generally opted to use laboratory rates (e.g., Gunter et al., 1997; Xu et al., 2003). In general, we know little about the proper rates and rate laws that are applicable to geological systems (Lasaga, 1998). However, a firm scientific basis for predicting reaction kinetics in natural environments is urgently needed to assure the reliability of the geochemical models used for the carbon sequestration program.

The funded research here attempts to resolve this **outstanding scientific issue**. The chemical, physical, and biological processes in the deep geological formation are complex and inter-related. Monitoring subsurface activities is costly. Thus, the results of the funded research represents a necessary step in **reducing cost** associated with geological carbon sequestration by developing mathematical models for evaluating and optimizing the injection program. Over the long-term, geological carbon sequestration will go through performance assessment evaluation processes, and as time progresses, the reaction kinetics problem is likely to occupy a more prominent position. Our results will provide crucial parameters for the performance assessment.

Feldspars (Fig. 1) are the most abundant silicate minerals and comprise over 50% of the volume of the earth's crust. When CO_2 is injected into geological formations, CO_2 will react with silicate minerals in the aquifers (such as in the case of the Frio sandstone, Texas, Weyburn, Canada, and the Sleipner projects mentioned above). The reactions will increase the pH of the brine, resulting in an enhanced solubility of CO_2 in brine, which is a desirable effect because it reduces the chance of CO_2 leakage to the surface.

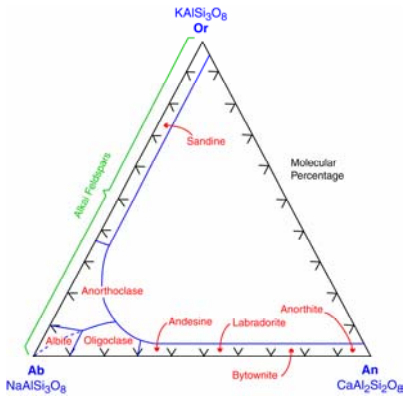

Figure 1. Chemical compositions and nomenclature of feldspars.

Dissolution of feldspars can also release Ca^{2+}, which can form carbonate precipitates. This is the most desired consequence of CO_2 injection because carbonate solids are immobile and are permanently stored in deep geological formations without the risk of seeping back to the surface. As pointed out by the NRC workshop report (NRC, 2003), this is a natural process of weathering. However, the key to the carbon sequestration program is an understanding of the reaction kinetics and how to accelerate the process.

Another consequence of silicate reaction after CO_2 injection is the change of porosities in the geological formation, which can alter the patterns of fluid flow and cause formation damage. STRAZISAR et al. (2003) again demonstrated that the magnitudes of porosity changes are closely related to the kinetic parameters used in the model.

In addition to the long-term controversy between field and laboratory rates, there is a general lack of experimental data at conditions pertinent to the geological carbon sequestration program. The reactions pertinent to geological carbon sequestration occur in about 50 to 150 ^{o}C, high CO_2 pressure, and in saline brines. Although high CO_2 concentrations might suggest pH lowering and more rapid dissolution of primary aluminosilicates, these conditions may enhance further the stability of clay minerals and carbonate minerals, with attendant effects on the overall reaction rate schemes. Moreover, it is not at all clear from available data whether high CO_2

concentrations in fluids act to catalyze or inhibit mineral dissolution/precipitation processes typical of or likely to be found in geologic terrains impacted by carbon sequestration.

There is a dearth of kinetic data relevant to geological carbon sequestration, and hence the need for experimental measurements.

Furthermore, we want to test experimentally the feasibility of using some unconventional CO_2 storage formations. Red sandstone beds are widespread worldwide and co-injection of SO_2 and CO_2 could reduce ferric iron to ferrous iron and form **iron carbonate** precipitates. One of the major costs of the carbon sequestration program is the capture and purification of CO_2 at point sources. If some impurities in flue gas, such as SO_2, can have beneficial use, it represents a major cost reduction to the program. Although theoretical calculations show great promise for this strategy (Knauss et al., 2002; Palandri and Kharaka, 2003), the redox reactions are dominated by kinetics and little experimental kinetic data are available.

With these goals in mind, we have devised an innovative experimental and theoretical interpretation program to address these urgent and significant outstanding scientific issues facing the carbon sequestration program.

2. Executive Summary

Currently, DOE is conducting pilot CO_2 injection tests to evaluate the concept of geological sequestration. One strategy that potentially enhances CO_2 solubility and reduces the risk of CO_2 leak back to the surface is dissolution of indigenous minerals in the geological formation and precipitation of secondary carbonate phases, which increases the brine pH and immobilizes CO_2. Clearly, the rates at which these dissolution and precipitation reactions occur directly determine the efficiency of this strategy. However, one of the fundamental problems in modern geochemistry is the persistent two to five orders of magnitude discrepancy between laboratory-measured and field derived feldspar dissolution rates. To date, there is no real guidance as to how to predict silicate reaction rates for use in quantitative models. Therefore, a firm scientific basis for predicting silicate reaction kinetics in CO_2 injected geological formations is urgently needed to assure the reliability of the geochemical models used for the assessments of carbon sequestration strategies.

This research project addresses this critical and urgent need of the carbon sequestration program. The research program is built upon the PIs' substantial previous work in the field of water-gas-rock interactions, including some work in the carbon sequestration program. Hence, the funded work can be easily integrated with the NETL in-house research, and NETL-sponsored programs of field tests of injecting CO_2 into deep geological formations (Frio sandstone, Sleipner, and Weyburn projects), and mineral carbonation and brine sequestration programs (NETL, Los Alamos, Albany Research Center).

During the first year of this three year project, the following accomplishments have been made:

1. We have successfully developed a sample preparation method and prepared reactants for experiments. The samples are free of fine particles, and have been characterized with electron microprobe and scanning electron microscope (SEM). These samples have been used in subsequent hydrothermal experiments.

2. We have used the state-of-the-art, atomic scale High Resolution Transmission Electron Microscope (TEM) to characterize the fresh reactants (before experiments), which establishes a baseline for characterizing the products from experiments. An amorphous layer of nanometer-thickness is found on the cleavaged feldspar surface as a result of sample preparation artifact (ion-milling). This finding is a significant step in the development of sample preparation protocols because it establishes the baseline for interpretation of experimental products. Our state-of-the-art Energy filtered TEM (EFTEM) microscopy has successfully mapped the chemical compositions of the unreacted feldspar surface. This establishes the baseline for analyzing feldspar surface chemistry for the reactant later in the project. These findings are new. The images are among the first obtained on the subject.

3. We have successfully completed three batch type feldspar dissolution experiments with duration from 26 to 79 days and obtained time series solution chemistry data. These data allow us to calculate feldspar dissolution rates as a function of time and saturation states.

The products from these experiments provide the opportunity to characterize the reacted mineral surfaces.

4. We have used SEM, TEM, and XPS to characterize the mineral products. SEM shows that the surfaces of reacted feldspar grains are covered with secondary clay particles. TEM study shows that they are sheet silicates. We are making significant progresses on using High Resolution TEM to characterize the mineral surfaces.

5. We have conducted substantial amount of geochemical modeling work on interpretation of experimental results. We are making good progress and are on target on this task.

In summary, we have met or exceeded the milestones during the first year. We anticipate that the second year will be a more fruitful year as our graduate students are already trained and results from the first year are ready for interpretation and publication. Overall, our results will help to resolve one of the major outstanding scientific issues facing the carbon sequestration program: the rates of chemical reactions in geological formations. The results will benefit the program by introducing the development of numerical performance assessment models, which will reduce the costs of monitoring and design.

3. Experimental

3.1. Sample Preparation

Orthoclase crystals having an average size of ~0.5 cm were purchased from the Wards Natural Sciences establishments, Inc. These crystals were handpicked, then ground with an agate mortar and pestle, and subsequently dry sieved. Finer grained material was discarded and coarser material was reground.

The size fraction between 50 and 100 μm was ultrasonically cleaned using acetone to remove fine particles. This treatment was repeated eight times on each aliquot for about 20 min per treatment. A devise shown in Fig. 2 was used to further removing the fines. The mixture of acetone and mineral powders in the measuring cylinder were gently stirred and a steady upswing flow was formed in the measuring cylinder which drove the fine particles out of the measuring cylinder and into the large beaker. The large particles were remained in the measuring cylinder. Scanning Electron Microscopy (SEM) shows that the fines are essentially removed (see Figure 5).

Figure 2. Device for removing the fine particles.

The grains were quickly washed several times with distilled water and then dried in a freezing drier overnight. Before experiments, the grains were put into an oven (105 ^{o}C) overnight to remove possible organic materials. The specific surface area of the cleaned powder was determined by N_2 gas absorption using the B.E.T. method.

3.2. Batch Experiments

The prepared feldspar grains were placed in a flexible gold reaction cell with detachable Ti-closure (Seyfried et al., 1987). This arrangement allows easy access to the reactants at the end of an experiment. More importantly, the flexible cell permits **on-line sampling of the aqueous phase at constant temperature and pressure** simply by adding water, in an amount equivalent to the sampled fluid, to the region surrounding the reaction cell (Fig. 3). These experimental data are generally superior to those derived from samples collected after the reactors are cooled down because backward reactions may occur during cooling.

The experiments using the flexible cell system were conducted at temperature of 200 °C and 300 bars. Fluid samples taken from the reactor at regular intervals were analyzed for all major and some minor dissolved components. Dissolved cations were analyzed by inductively coupled plasma mass spectrometry (ICP-MS), while anions were analyzed by ion chromatography.

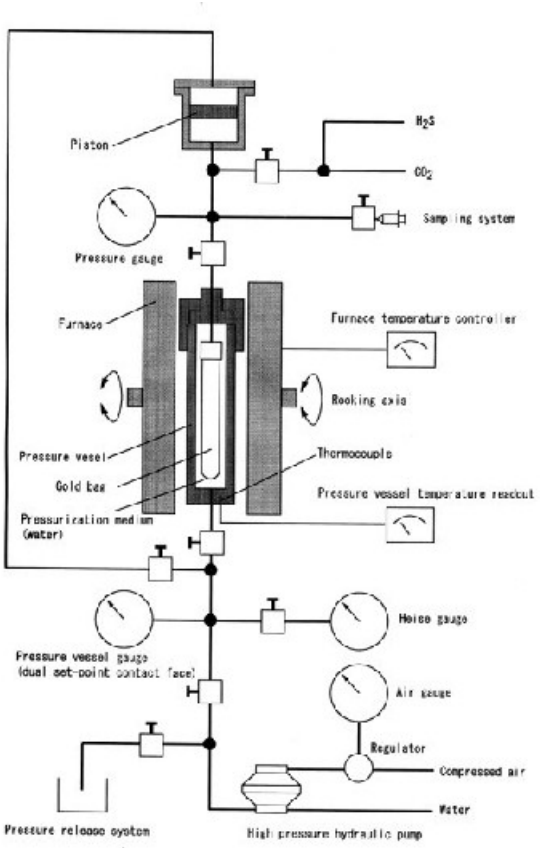

Figure 3. Schematic illustration of the flexible cell reaction system (Seyfried et al., 1987), which is being used for the mineral dissolution/precipitation rate studies.

The measured fluid chemistry including pH, when considered with distribution of aqueous speciation, taking explicit account of mass balance, mass action and charge balance constraints, together with constrains imposed by the revised HKF equation of state (Shock and Helgeson, 1988; Shock et al., 1989; Johnson et al., 1992; Shock et al., 1992; Sverjensky et al., 1997), permits calculation of ion activities of dissolved species.

3.3. Electron Micro Beam Characterization of Reactants and Products

Reactants and products were investigated by an array of sophisticated techniques: gas adsorption (B.E.T surface area), SEM (phase relationships and surface morphology), electron microprobe, and XPS (surface chemistry), as well as High-resolution TEM (structure and chemistry).

Scanning Electron Microscopy (SEM) was conducted with a Philips XL 30 Field Emission Gun (FEG) SEM and an RJ Lee Instruments Personal SEM. The SEM has secondary and back scattered electron detectors for imaging, as well as an energy dispersive X-ray spectrometer with an EDAX ultrathin window CDU LEAP detector capable of analyzing light

elements down to carbon. Feldspar grains were made into double-sided, polished petrographic thin-sections. The drill cutting samples were mixed with epoxy, secured into 1-inch phenol rings and gently polished to a smooth, flat surface. For grain mounts, sand grains were sprinkled onto double-sided tape. Samples were coated with a layer of carbon before SEM analysis. The compositions of feldspars were determined by wavelength dispersive X-ray spectroscopy using a CAMECA SX50 electron microprobe.

TEM observations were performed using a Philips CM300FEG microscope operated at 295 kV and a JEOL 2010 microscope operated at 200 kV. X-ray microanalyses were performed using a Philips EM 420 microscope equipped with an Oxford Si (Li) energy-dispersive X-ray system (EDS) and analytical software Desk Top Spectrum Analyzer (DTSA) from the National Institute of Standards and Technology. Data reduction was carried out using the standard Cliff-Lorimer method implemented in the DTSA.

Two TEM sample preparation methods were used, crushing and ion milling. In the first method, samples were ground in an agate mortar, suspended in ethanol, and then dropped on holey carbon film supported by a standard Cu TEM grid and air-dried. In the second method, specimens were prepared by cutting from petrographic thin sections and mounted onto single-hole Cu grids. Cu grids were mounted on the focus area, and the sample was further thinned to ~100 nm, using an ion beam. Finally, a very thin carbon film was coated onto the ion milled samples.

4. Results and Discussion

4.1. Solution Chemistry from Batch Experiments

Experiments using the flexible reaction cell system were conducted at 200 °C and 300 bars. These experiments involved the K_2O-Na_2O-Al_2O_3-SiO_2-H_2O-HCl±CO_2 system. The plan for each chemical system was to assess reaction progress with and without dissolved CO_2, which served as a source of acidity. In the absence of dissolved CO_2, acidity was added directly in the form of excess dilute HCl.

Time series fluid chemistry for both chemical systems is listed in Tables 1, 2, and 3. These results will allow assessment of mineral dissolution and precipitation processes as a function of dissolved CO_2, mineral saturation state, and temperature.

Table 1. Time-dependent changes in the composition of major dissolved species in CO_2-bearing aqueous fluid coexisting with K-feldspar at 200 ^oC and 300 bars. The overall analytical error for dissolved species is ±5%. In-situ pH is calculated from distribution of aqueous species calculations at the temperature and pressure of the experiment using constraints imposed by major element concentrations and pH values measured at 25 ^oC.

Sample	Time (days)	SiO_2	K^+	Na^+	NH_4^+	Cl^-	CO_2(aq)	pH (25^oC)	In-situ pH (200^oC)
				(mmol/kg solution)					
#1	1	0.40	196.31	0.26	0.06	199.22	47.90	4.3	4.99
#2	6	1.88	194.30	0.45	0.11	196.51	44.47	4.5	5.21

#3	13	2.30	195.35	0.93	0.13	197.48	45.83	5.0	5.73
#4	20	2.42	196.19	1.41	0.12	199.40	45.35	5.1	5.83
#5	27	2.49	195.40	0.97	0.23	198.77	45.17	5.1	5.83

Table 2. Time-dependent changes in the composition of major dissolved species in non-CO_2-bearing aqueous fluid coexisting with K-feldspar at 200 ^oC and 300 bars. The overall analytical error for concentration measurements is ±5%. In-situ pH is calculated from distribution of aqueous species calculations at the temperature and pressure of the experiment using constraints imposed by major element concentrations and pH values measured at 25 ^oC.

Sample	Time (days)	SiO_2	Al^{3+}	K^+	Na^+	Ca^{2+}	NH_4^+	Cl^-	pH (25^oC)	In-situ pH (200^oC)
				(mmol/kg solution)						
Starting	0	-	-	203.99	-	3.72	0.16	198.30	3.0	
#1	1	0.31	0.007	202.77	0.42	0.12	0.12	197.53	3.2	3.27
#2	9	1.46	0.003	201.06	1.13	0.21	0.20	198.65	3.5	3.57
#3	19	1.70	0.08	197.77	2.04	0.43	0.23	196.82	4.1	4.13
#4	34	1.35	0.03	204.31	1.86	0.16	0.29	197.90	4.2	3.92
#5	57	4.20	0.15	197.06	3.82	0.31	0.32	199.66	4.8	4.60
#6	78	3.76	0.06	197.53	1.91	0.35	0.16	199.20	4.7	4.60

Table 3. Time-dependent changes in the composition of minor and trace dissolved species in non-CO_2-bearing aqueous fluid coexisting with K-feldspar at 200 ^oC and 300 bars (see Table 2). The overall analytical error for concentration measurements is ±5%.

Sample	Li	Mg	Cr	Fe	Mn	Co	Ni	Cu	Zn	Rb	Sr	Cs	Ba
							(ppm)						
Starting	0	0.02	0	0	0	0	0	0.01	0.02	0.04	0.03	0	0.06
#1	0.07	0.22	0	0	0.03	0	0.07	0.35	0.19	0.17	0.18	0.02	0.60
#2	0.01	0.22	0	0.82	0.04	0.03	0.10	0.83	0.62	0.15	0.62	0.01	0.58
#3	0	0.18	0	0.74	0.04	0.02	0.03	0.08	0.28	0.14	0.71	0	0.59
#4	0.04	0.25	0	0.55	0.04	0.02	0.01	0.10	0.29	0.16	0.76	0.02	0.58
#5	0.01	0.20	0	0.40	0.04	0.02	0.02	0.16	0.31	0.15	0.84	0.01	0.59
#6	0	0.33	0	0.22	0.04	0.02	0	0.21	0.35	0.14	0.89	0.01	0.56

The CO_2-bearing experiment in the K_2O-Na_2O-Al_2O_3-SiO_2-H_2O-HCl system (Table 1) predictably resulted in relatively high initial pH, and thus, reaction commenced in the muscovite field of stability (Fig. 4). Dissolution of K-feldspar moved the fluid relatively rapidly to near the muscovite-K-feldspar join, at which point the experiment was terminated, since full equilibrium was achieved. As noted, the second experiment in this chemical system involved a more acidic starting fluid owing to the presence of excess HCl. Thus, this experiment commenced in the diaspore field of stability and progressed relatively slowly, although far removed from K-

feldspar stability field. Once in the muscovite field the fluid chemistry revealed a perturbation, apparently induced by the diaspore buffering. The cause of the negative slope in K^+/H^+-SiO_2(aq) space likely involved complex rate relations involving diaspore dissolution, K-feldspar dissolution and muscovite precipitation. Apparently, formation of diaspore during early stages of the experiment affects significantly subsequent reaction progress and rates of attainment of overall fluid-mineral equilibria. Once all the diaspore has been consumed in the formation of muscovite, the reaction can proceed to the muscovite-K-feldspar equilibrium, as observed (Fig. 4). Subsequent reaction path modeling likely will allow provisional constraints to be placed on the amount of diaspore needed to account for the observed experimental data.

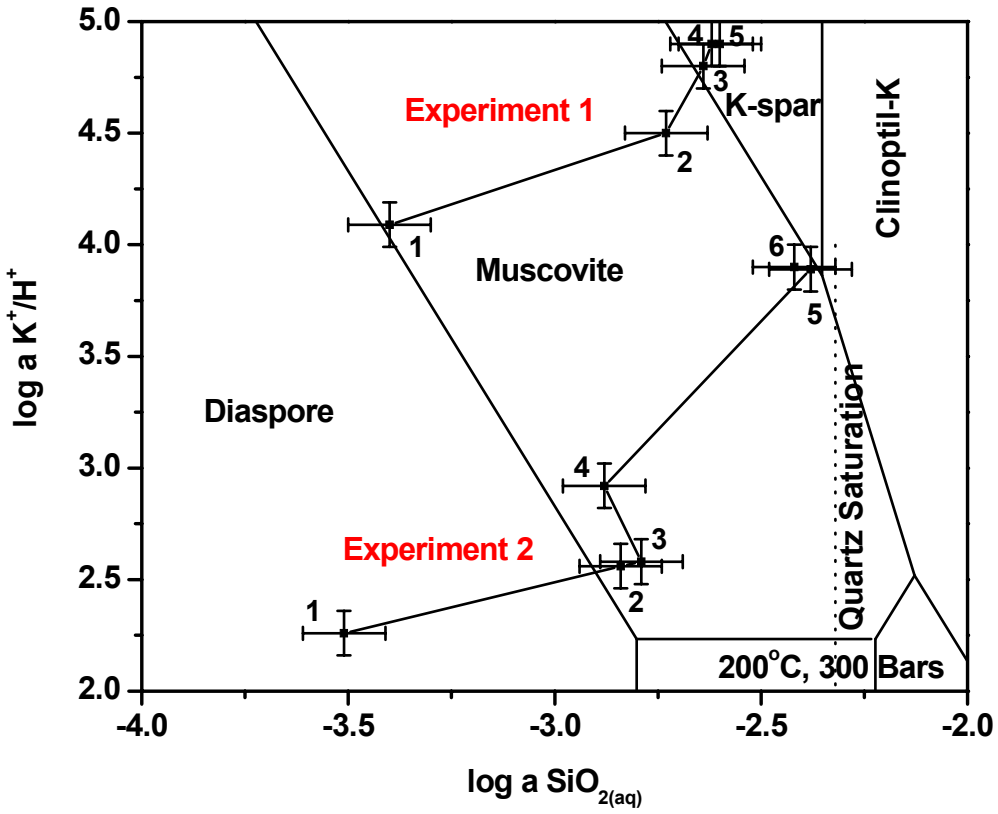

Fig. 4. Activity diagram in the K_2O-Al_2O_3-SiO_2-H_2O-HCl±CO_2 system at 200 °C and 300 bars. These data suggest that the more acidic system involving excess HCl results in formation of diaspore, which causes a correspondingly delay in attainment of full equilibrium. Thus, experimental and theoretical results will help to constrain the role of diaspore on overall rate and processes of mass transfer in this geologically important system.

Indeed, preliminary geochemical modeling (as a part of Task 3) suggests coexistence of K-feldspar and muscovite at the end of both experiments in the K_2O-Al_2O_3-SiO_2-H_2O-HCl±CO_2

system. In effect, the time dependent release of dissolved silica serves well as a proxy for assessing reaction rates.

The surface chemistry of K-feldspar was analyzed using X-ray photoelectron spectroscopy (XPS), before and after the CO_2-bearing experiment ("Experiment 1", Fig 4). Results show that the K/Al and Al/Si mole ratios changed significantly from 0.66 to 0.39, and 0.37 to 0.75, respectively (Table 4). The decrease of Al/Si and the increase of K/Al of K-feldspar surface following the experiment imply formation of muscovite, which is consistent with preliminary geochemical modeling results.

Table 4. XPS surface composition results* of K-feldspar from "Experiment 1" (Fig. 4) in comparison with theoretical values for K-feldspar and muscovite. The data indicate a significant decrease in K/Al consistent with muscovite-like mineralization at the K-feldspar-fluid interface.

	K	Al	O	Si	K/Al	Al/Si
	mole%				mole ratio	mole ratio
Starting K-feldspar	5.7	8.7	62.3	23.4	0.66	0.37
K-feldspar Product	5.3	13.6	62.9	18.2	0.39	0.75
K-feldspar	7.7	7.7	61.5	23.1	1	0.33
Muscovite	5.3	15.8	63.2	15.8	0.33	1

*Each result reflects the average value of 4 measurements from different K-feldspar grains within the same sample.

These results allow for calculations of overall feldspar dissolution rates and their variation with time. The dissolution rates of K-feldspar (moles of K-feldspar/cm^2/s) were calculated based on the Si concentration variation (Table 5). The time dependent release of dissolved silica serves well as a proxy for assessing reaction rates.

Table 5 Dissolution rates based on Si concentration variation

Experiment 1		Experiment 2	
Time duration	Rate (moles/cm^2/s)	Time duration	Rate (moles/cm^2/s)
0-1 day	2.338×10^{-14}	0-1 day	2.416×10^{-14}
1-6 day	1.730×10^{-14}	1-9 day	1.120×10^{-14}
6-13 day	3.507×10^{-15}	9-19 day	1.871×10^{-15}
13-20 day	1.002×10^{-15}	19-34 day	-1.820×10^{-14}
20-27 day	5.845×10^{-16}	34-57 day	9.658×10^{-15}
		57-78 day	-1.630×10^{-15}

Note: Ratios of surface area to solution for experiment 1 and experiment 2 are 1320 $cm^2/g \times 2$ g/ 0.04 L = 66,000 cm^2/L and 1320 $cm^2/g \times 1.5$ g / 0.04 L = 49,500 cm^2/L, respectively. The rate calculation is normalized to that of 1 L solution.

4.2. Electron Microbeam Characterization of Reactants before Batch Experiments

At this stage of the project, most work that has been performed includes using a new Filed Emission Gun (FEG)-Scanning Electron Microscope (SEM) and High Resolution Transmission Electron Microscope (HRTEM) to characterize the reactants. This work has

established a baseline for comparison with results on reactants and products after experiments. As the project progresses, more work will move toward characterization of the reaction products.

4.2a. SEM Results for Reactants

The following pages are SEM photos, which primarily show that (1) the fines were successfully removed during sample preparation; and (2) there are exsolution laminae in the feldspars, which must be taken into account of in the interpretation in the experimental results. Non-stoichiometric dissolution, meaning dissolved constituents not proportion to that in the original solids, can be either interpreted as containing laminae with different composition or preferential leaching of chemicals in the surface layers of the reactants. The photomicrographs were obtained using a FEI Quanta 400 FEG Environmental Scanning Electron Microscopy equipped with a PGT Spirit EDS detector. A feldspar grain is particularly chosen for PTS mapping (Figure 9) with EDS detector. K and Na map clearly show the exsolution feature of the K-feldspar.

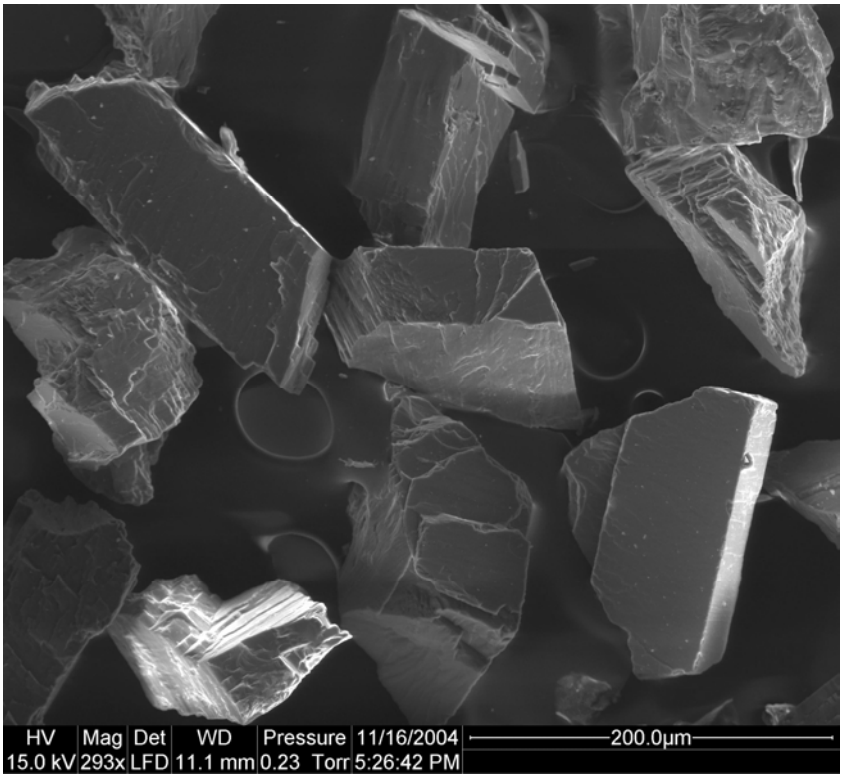

Figure 5. SEM micrograph, taken at 293X showing that feldspars used in the hydrothermal reaction experiments, are free from extra-fine particles and have angular shapes. This morphology will be compared to reacted feldspars (see Fig. 10).

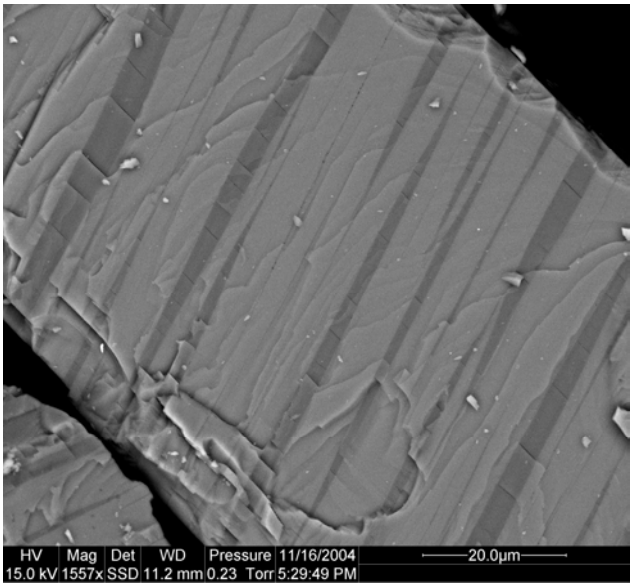

Figure 6. SEM micrograph of orthoclase, taken at 1557X, showing presence of an exsolution lamella, which we need to consider in the interpretation of experimental results.

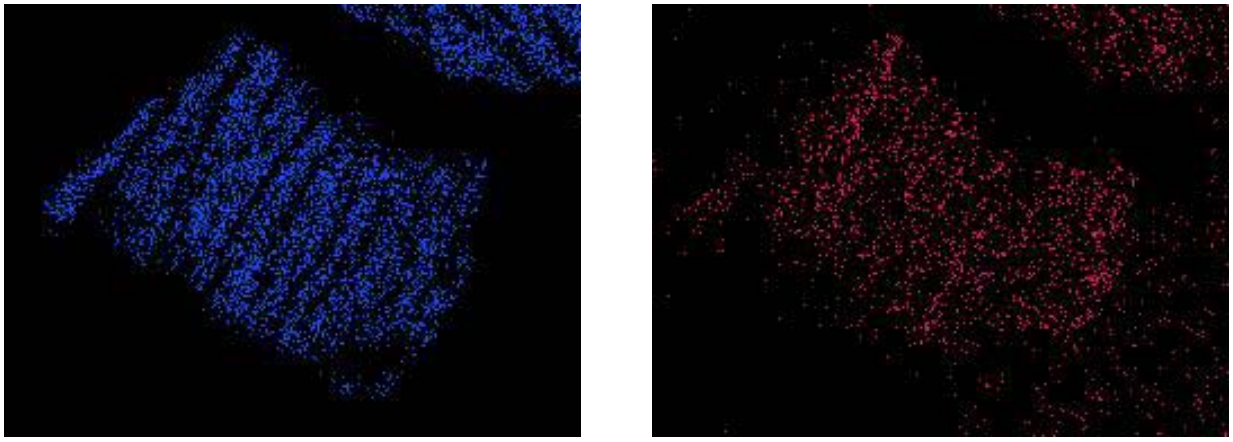

a b

Figure 7. K(a) and Na (b) PTS EDS map of the orthoclase particle in Figure 6 showing the exsolution feature of K-feldspar. The accumulation time of Na-map is longer than that of K-map to get enough resolution of Na distribution.

4.2b. TEM Results for Reactants

We have also used atomic scale TEM to characterize the reactants. Specimens for HRTEM observation were prepared by ion milling. K-feldspar crystal was crushed using a nipper. The resulting fragments of crystal with a well developed cleavage surface were glued on a glass slide, grinded, polished until it was 20 μm thick, and mounted on a Cu TEM grid. We thinned the samples with a Gatan Dual Ion Mill Model 600 using Liquid N_2. Initial thinning was at a voltage

of 5 kV and an incident ion-beam angle of 18 degree, followed by gentler milling at a voltage at 3 kV and an incident angle of 16 degree. The ion milled specimens were lightly carbon coated. HRTEM and Energy-filtered TEM (EFTEM) were carried out with Philips CM300FEG microscopes, operating at 295 kV (point-to-point resolution 0.2 nm)

Amorphous material ranging from several to 35 nm in thickness occurs on surface of ion-milled K-feldspar and cleavage surface (Fig. 8). Thickness of amorphous layer is variable, depending on ion milling instrument and ion-milling conditions such as incident ion-beam angle and voltage. EFTEM shows that Si and Al concentration in unaltered amorphous materials and crystalline feldspar are not visibly different (Fig. 9). It appears that the amorphous layer was either formed by radiation damage, or deposition of spattered materials from K-feldspar, or the both.

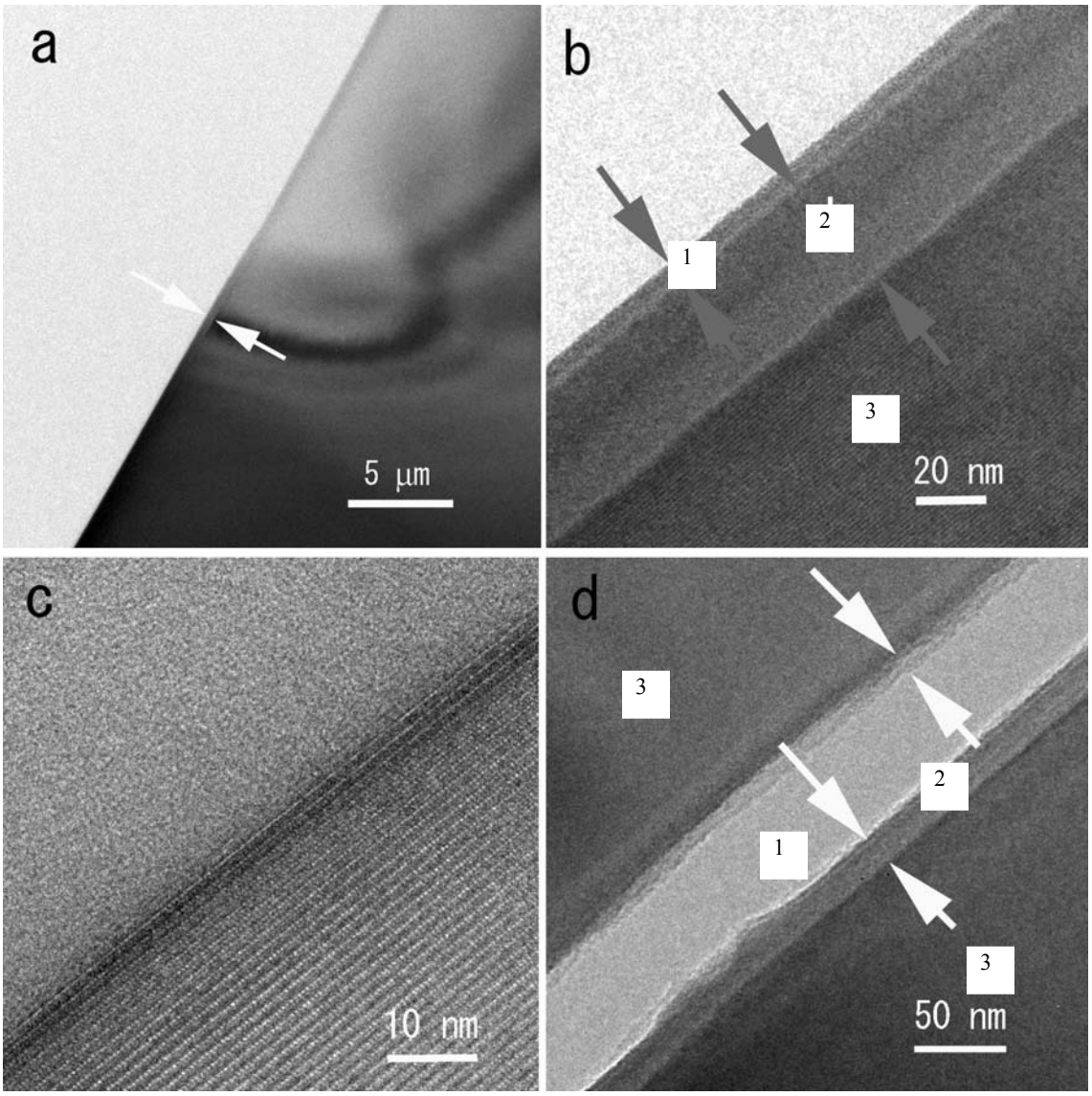

Figure 8. TEM images of an ion-milling sample (without any other treatments) (a) the low magnification diagram. Stripes are crystal bending. Arrows indicate the boundaries of phase transition. (b) high magnification diagram of crystal boundary of (a). The layer labeled as "1" is likely to be carbon contamination. The amorphous layer is labeled as "2". The orthoclase crystal is labeled as "3". Arrows show the boundaries of phase transition. (c) Enlargement of 2 and 3 of (b). (d) Cleavage of orthoclase crystal caused by ion-milling. The cleavage is labeled as "1". The amorphous layer is labeled as "2". The orthoclase crystal is labeled as "3". Arrows show the boundaries of phase transition.

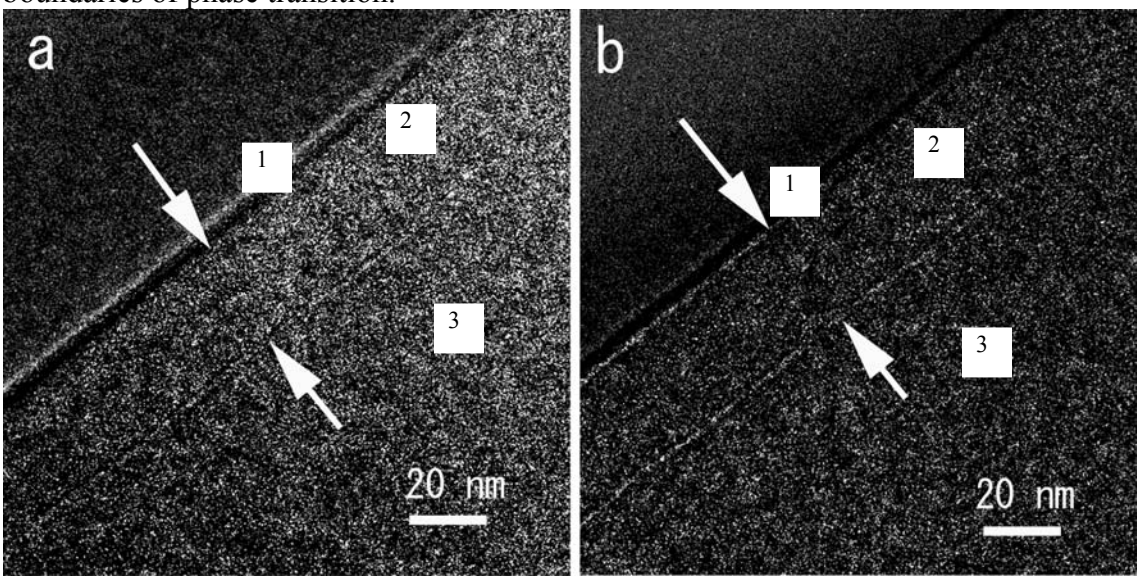

Figure 9. EFTEM figure of Fig.15b. Labels "1", "2", and "3" are the same as in Fig.15b. (a) Si map. (b) Al map. Si and Al concentrations in unaltered amorphous materials and crystalline feldspar are not visually different.

4.2c. Electron Microprobe Analysis of Reactants

The composition of orthoclase specimen was determined by electron microprobe analysis (EMPA CAMECA SX 50) at an operating voltage of 15 kV and a beam current of 5 nA. The values of 8 measurements on the starting sample are given in Table 6.

Table 6. The composition and chemical formula of starting orthoclase

Oxide	SiO_2	Al_2O_3	Na_2O	FeO	K_2O	CaO	Total
wt%	66.706	21.37	8.986	0.128	1.64	1.042	99.872
	63.317	19.696	3.792	0.042	9.626	0.444	96.917
	62.483	19.187	1.834	0.046	13.292	0.018	96.86
	62.468	19.209	1.259	0.078	14.32	0.031	97.365
	62.948	18.896	1.214	0.075	14.282	0	97.415
	62.331	19.143	1.311	0.076	14.158	0.011	97.03
	62.315	19.068	1.525	0.068	13.732	0.018	96.726
	66.807	20.415	3.402	0.114	11.897	0.231	102.866
wt% average	63.67188	19.623	2.915375	0.078375	11.61838	0.224375	98.13138
Cations per 8	2.929	1.106	0.765	0.005	0.092	0.049	4.946

Oxygen atoms	2.949	1.081	0.342	0.002	0.572	0.022	4.968
	2.954	1.069	0.168	0.002	0.802	0.001	4.996
	2.951	1.069	0.115	0.003	0.863	0.002	5.003
	2.968	1.05	0.111	0.003	0.859	0	4.991
	2.953	1.069	0.12	0.003	0.856	0.001	5.002
	2.956	1.066	0.14	0.003	0.831	0.001	4.997
	2.954	1.064	0.292	0.004	0.671	0.011	4.996
Cations average	2.95175	1.07175	0.256625	0.003125	0.69325	0.010875	4.987375

4.2d. BET Surface Area of Reactants

Surface area of fresh feldspar samples was analyzed using a Coulter SA 3100 Surface Area and Pore Size Analyzer. A specific surface area of 0.132 m^2/g was measured by nitrogen gas adsorption using the BET method.

4.3. Microbeam Analysis of Products from Batch Experiments

In addition to the characterization of the **reactants** using a variety of microbeam technologies, we have also made solid progress on characterization of **products** from the batch experiments. It should also be noted that during the first year, we also made accomplishments on educating our graduate students working on this project, training them to use the microbeam technologies necessary for the research.

X-ray diffraction (XRD) measurements were conducted to analyze the mineralogical compositions of the products. However, the quantities of alteration products are too small to be detected by XRD. XRD can only detect materials about >5%. We expect the secondary mineral precipitate in our samples are <1%. However, the XRD work is necessary due diligence.

Important progresses have been made on graduate student training and education. Ph.D. graduate student Peng Lu has been supported by this grant. He has been trained to use Scanning Electron Microscope housed at Indiana University through a semester long seminar course. He is permitted to operate SEM himself. This will greatly facilitate the subsequent work for Task 2. Mr. Peng is going to take a TEM course in the fall. Below is a summary of some of his work.

SEM photomicrographs of products following batch dissolution experiments (Figure 10) show dissolution etch pits, demonstrating that dissolution has occurred. Larger and deeper etch pits and more secondary minerals are observed on the feldspar grains after Experiment 2 than after Experiment 1, showing that Experiment 2 reacts more extensive than Experiment 1.

Two kinds of secondary minerals, one shaped as needles and the other as hexagon, are visible on the feldspar surface (Figure 10). TEM results show that the secondary minerals are sheet silicates, but did not identify the specific mineral species because the resolution of the TEM at Indiana University campus is too low. Arrangement has been made to use the high resolution TEM at Carnegie Mellon University, Purdue University, and Johns Hopkins University. Now, the graduate student is trained, we expect considerable progress in the second year.

Experiment 1

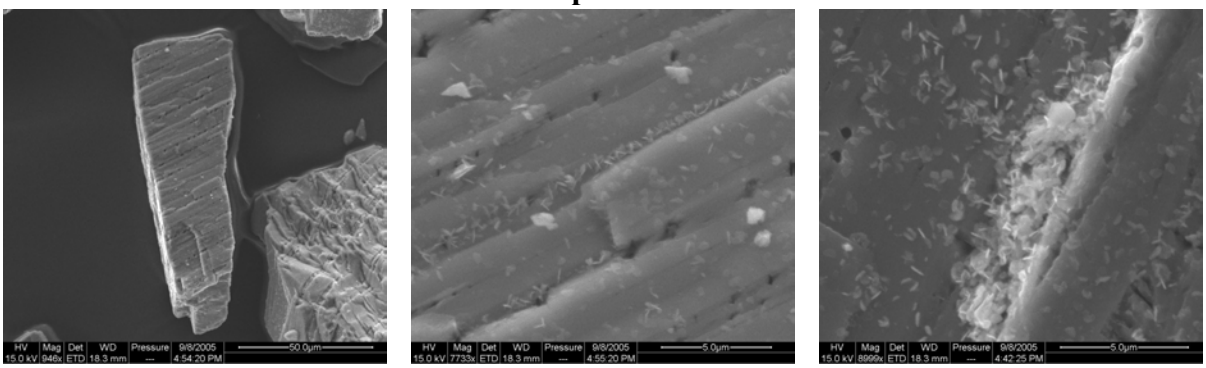

Experiment 2

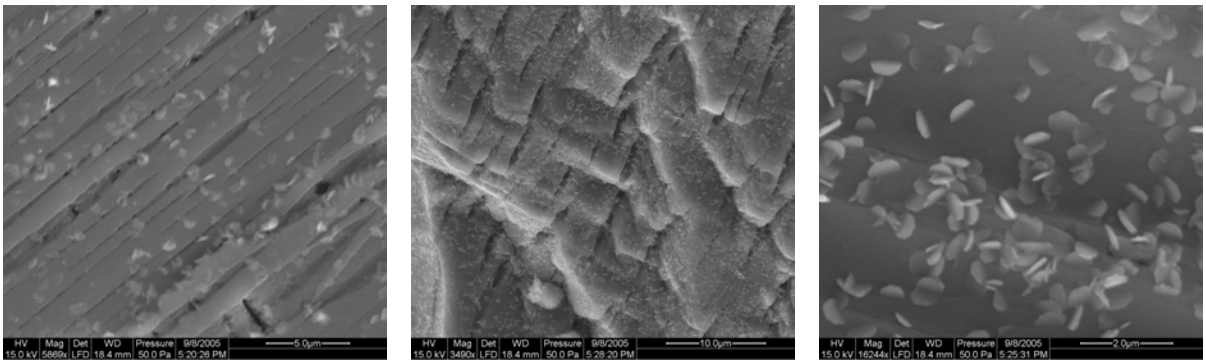

Figure 10. Scanning electron microscopy images of K-feldspar after dissolution Experiments 1 and 2. Etch pits and two kinds of secondary minerals, one shaped as needles and the other as hexagon (kaolinite, muscovite?), are visible on the feldspar grains. Larger and deeper etch pits and more secondary minerals are observed on the feldspar grains after Experiment 2 than after Experiment 1, showing that Experiment 2 reacts more extensive than 1.

4.4. Geochemical Modeling

Two types of geochemical models are used for design and interpretation of experiments. Although the methodology of these geochemical models is well established, the utilization of them in interpretation of experimental results is innovative.

4.4a Inverse Mass Balance Modeling

Inverse mass balance modeling (inverse modeling) is fundamentally based on the simple relationship: initial water + reactants = final water + products, and uses the measured differences in "final water-initial water" to make deductions about reactants and products. In practice, inverse modeling is used to find out the mass transfer reactions responsible for the observed water chemistry differences between two sampling points along a flow path (Plummer, 1990; Zhu and Anderson, 2002). When important assumptions are satisfied for the models (i.e. initial and final water analysis represent flow along the same path; dispersion and diffusion do not affect water chemistry prominently; a chemical steady state prevailed during time of interest; the mineral phases used in the calculation are or were in the aquifer) (Chen and Anderson, 2002), the

evolution of water chemistry can be largely attributed to dissolution and/or precipitation as well as ion exchange reactions. The inverse modeling reflects an effort of integrating a more comprehensive set of elemental and mineralogical data into a different type of modeling. Unlike reaction path modeling, which look at the degree of agreement between modeled results and field measurements for the same "end" point, inverse modeling analyzes the differences between "start" and "end" points along the path and come up with a set /sets of reactions that account(s) for the "net" changes. In many cases, more than one set of reactions appears to be adequate, and a further step would be a coupled analysis of the model results with actual mineralogical observations, saturation indices calculation, and chemical kinetic considerations in order to find the most realistic set(s) of results. Parkhurst (1997) found that inclusion of uncertainty analysis can reduce the number of phases needed to reproduce the net chemical changes and thereby reduce the number of models.

Our graduate student has taken a course Geochemical Modeling by Chen Zhu. He will perform the modeling in spring 2006.

4.4b. Reaction–path Modeling

The second type of geochemical model is the *reaction-path model*. Reaction path models calculate a sequence of equilibrium states or steady states involving incremental or step-wise mass transfer between the phases within a system, or incremental addition or subtraction of a reactant from the system (Helgeson, 1968; Helgeson et al., 1969). The calculated mass transfer is based on the principles of mass balance, partial and local equilibrium, and reaction kinetics.

Feldspar hydrolysis is the system in which (Helgeson, 1968) developed the reaction-path modeling approach. Although the original example was based on local and partial equilibrium (Helgeson, 1968; Helgeson et al., 1969; Helgeson, 1979). HELGESON and MURPHY (1983) added feldspar dissolution kinetics into the model. LASAGA (1998) further showed that different reaction paths will result from different relative rates of feldspar dissolution and secondary mineral precipitation.

The computer code The Geochemist' Workbench™ was used for preliminary modeling study. Figure 11 shows the reaction paths we calculated from our preliminary modeling study. In the model calculation, we assume equilibrium among aqueous species, but feldspar dissolution and clay product precipitation are controlled by kinetics. The computer code PHREEQC (Parkhurst, 1999) was used for the rest of simulations. PHREEQC allows for flexible programming for any type of rate laws.

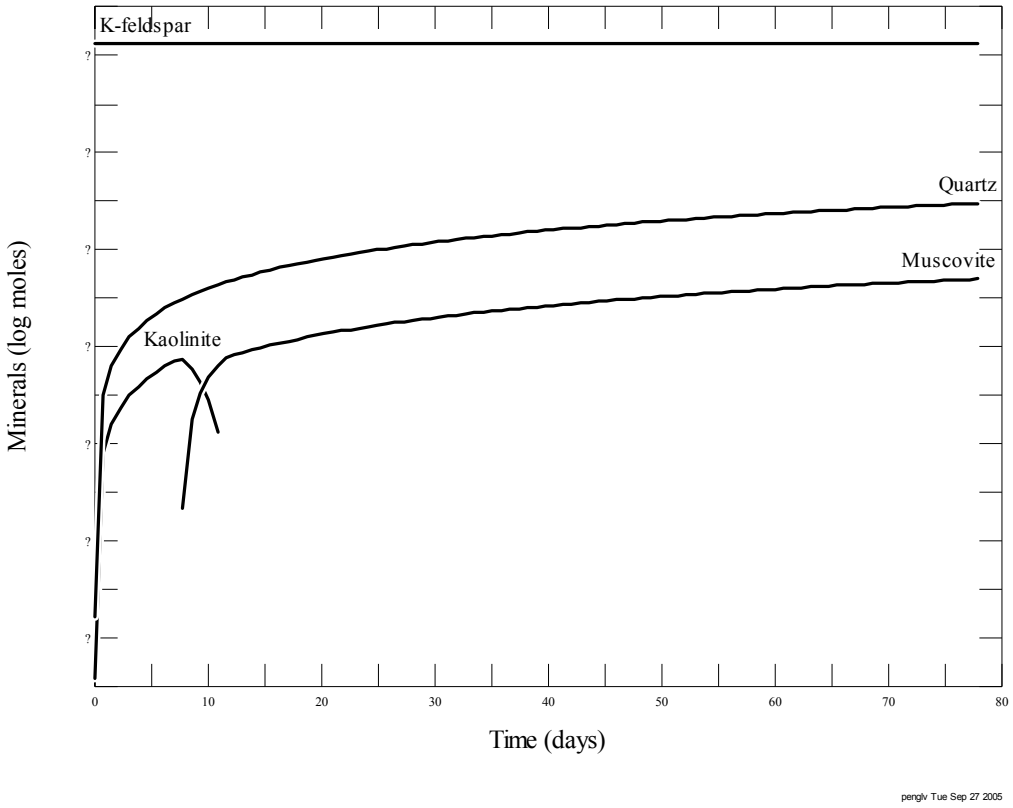

Figure11. Preliminary modeling of Experiment 2.

A significant amount of modeling work has been performed to interpret the batch dissolution experimental data. We are at the stage that we experiment different rate laws to evaluate how these rate laws affect the simulation of experiments.

Rate laws

Lasaga (1998) gave the general rate law for heterogeneous reactions,

$$Rate_j = \frac{1}{S_j}\frac{dN_j}{dt} = k_j a_{H^+}^{n_{H^+}} g(I) \prod_a a_i^{n_i} f(\Delta G_r) \qquad (1)$$

where $Rate_j$ is the rate of dissolution of the jth mineral, N_j denotes to the moles of mineral j, k_j the respective rate constant (mol s^{-1} m^{-2}), and S_j the reactive surface area of the jth mineral (m^2 L^{-1} or m^2 g^{-1}). a_H+ denotes the activity of hydrogen in the aqueous solution, and hence this term accounts for the well-noted pH dependence of dissolution rates. The term g(I) accounts for

possible ionic strength dependence of the rates. The term $\prod_a a_i^{n_i}$ incorporates the catalytic and inhibitory effects of all aqueous species other than H^+, e.g., Al (Oelkers, 1994).

The temperature dependence of the dissolution and precipitation rates is significant and is typically expressed using the Arrhenius equation

$$k = Ae^{-Ea/RT} \qquad (2)$$

where Ea is Arrhenius activation energy, and A is pre-exponential factor.

Blum and Stillings (1995) recommended a value of 51.7 kJ/mol of activation energy for K-feldspar, which they derived from acidic solution dissolution rates at various temperatures. A rate constant for K-feldspar of $1\times10^{-12.5}$ mol $s^{-1}\cdot m^{-2}$ is used at 25 °C (see Blum and Stillings, 1995), based on which a rate constant of $1\times10^{-9.15}$ at 200 °C is obtained. There is little knowledge of the proper rate laws for the precipitation reactions. Additionally, experimental clay precipitation rate data are rare (Nagy and Lasaga, 1992; Burch et al., 1993), and even clay dissolution rate data are scarce (Nagy, 1995; Cama J., 2000). The common practice is to either use the same rate constant derived from dissolution experiments or set one order of magnitude slower than dissolution reaction (Xu et al., 2003). Rate constants for kaolinite and muscovite are $1\times10^{-13.28}$ and $1\times10^{-13.07}$ at 25 °C, respectively (see Blum and Stillings, 1995). Activation energies of 43.1 kJ/mol for kaolinite at pH 2 and 22 for muscovite at acid solution from Nagy (1995) are used to derive rate constants at higher temperatures.

With little knowledge of surface areas for precipitates, we introduce an effective rate constant *k**, where $k_j^* = k_j S_j$. The feldspar surface area in the models is 6.6 m^2/L for Experiment 1 and 4.95 m^2/L for experiment 2, which is based on the BET specific surface area of 0.132 m^2/g and fluid/mineral ratios. The effective rate constants for K-feldspar are 4.67×10^{-9} for Experiment 1 and 3.50×10^{-9} for Experiment 2. Effective rate constants for secondary minerals are 2.15×10^{-10} for kaolinite in experiment 1, 1.61×10^{-10} in Experiment 2, 1.50×10^{-11} for muscovite in Experiment 1, 1.12×10^{-11} in Experiment 2, respectively.

As shown below, the surface areas of feldspars do not change much during the model simulation because only a small amount of feldspar is dissolved before reaching equilibrium. That is similar to what found by Helgeson and Murphy (1983) and Steefel and van Cappellen (Steefel, 1990). A common practice in treating time variant surface area is the assumption of the surface area is the function of

$$S_j = S_j^o \left(\frac{m_0}{m_j} \right)^{\frac{2}{3}}, \qquad (3)$$

where S^o the initial surface area of the jth mineral, m_0 is the initial moles of reactant, and m_j is the moles of reactant at a given time (e.g. Parkhurst, 1999). We adopted a constant surface area for feldspars, as in Helgeson and Murphy (1983) and Steefel and van Cappellen (Steefel, 1990), because their surface areas do not practically change during simulations. By introducing

effective rate constants for kaolinite and muscovite in terms of relative values to the feldspar k^*, we essentially also assume fixed surface areas for clay precipitates. In light of Eqn (3), the small k^* for clay minerals, introduced in the models, may represent the small surface areas in the beginning of the reactions.

We are constructing our reaction-path models in a step-wise fashion: first construct a model with K-feldspar kinetics only; and then add kaolinite, muscovite, etc., as the kinetic minerals. A total of 8 aqueous species, Al^{3+}, K^+, H_4SiO_4, Ca^{2+}, Cl^-, Na^+, NH_4^+ and H^+, and 6 minerals, K-feldspar, kaolinite, muscovite, Quartz, gibbsite and diaspore are included in the water-mineral system.

The initial solution in the reaction-path model is the experiment data (Figure 4). In all scenarios, homogeneous equilibrium is assumed in the aqueous solution. Activity coefficients for charged aqueous species were calculated from the WATEQ extended Debye-Hückel equation fitted to mean salt NaCl activity coefficients (Truesdell, 1974). For neutral species, the activity coefficients were assumed to be unity.

We found that temporal evolution of solution chemistry follow different paths for different relative rates. These calculations thus demonstrate that monitoring the reaction progress experimentally may give information about the relative rates and rate laws.

5. Conclusions

This research project addresses some critical and urgent needs of the carbon sequestration program. The research program is built upon the PIs' substantial previous work in the field of water-gas-rock interactions, including some work in the carbon sequestration program. Hence, the funded work can be easily integrated with the NETL in-house research, and NETL-sponsored programs of field tests of injecting CO_2 into deep geological formations (Frio sandstone, Sleipner, and Weyburn projects), and mineral carbonation and brine sequestration programs (NETL, Los Alamos, Albany Research Center). Zhu has regular contact or formal/informal collaboration with many of the principal investigators in these programs.

Specially, during the first year of the three year project, we have accomplished the followings:

- We have successfully developed a sample preparation method and prepared reactants for experiments. The samples are free of the fines, and have been characterized by electron microprobe and scanning electron microscopy (SEM). In particular, we have used the state-of-the-art, atomic scale High Resolution Transmission Electron Microscope (TEM) to characterize the fresh reactants (before experiments), which establishes a baseline for characterizing the products from experiments. An amorphous layer of nanometer-thick is found on the cleavaged feldspar surface as a result of sample preparation artifact (ion-milling). This finding is a significant step on development of sample preparation protocols because it establishes the baseline for interpretation of experimental products. Our state-of-the-art Energy filtered TEM (EFTEM) microscopy has successfully mapped the chemical compositions of the unreacted feldspar surface. This establishes the baseline for analyzing feldspar surface chemistry for the reactant later in the project;

- We have successfully completed three batch type feldspar dissolution experiments and obtained time series solution chemistry data. The products from these experiments are being analyzed (see below).

- We have made significant progresses on characterization of the reaction products by using SEM, TEM, and XPS.

- We have conducted substantial amount of geochemical modeling work on interpretation of experimental results. We are making good progress and are on target on this task.

In summary, we have met or exceeded the milestones during the first year. We anticipate that the second year will be a more fruitful year as our graduate students are already trained and results from the first year are ready for interpretation and publication. Overall, our results will help to resolve one of the major outstanding scientific issues facing the carbon sequestration program: the rates of chemical reactions in geological formations. The results will benefit the program by introducing the development of numerical performance assessment models, which will reduce the costs of monitoring and design.

References Cited

Blum A. and Stillings L. (1995) Feldspar dissolution kinetics. In *Chemical Weathering Rates of Silicate Minerals*, Vol. 31 (ed. S. L. Brantley), pp. 291-346. Mineralogical Society of America.

Bradley R. S. (2001) Many citations support global warming trend. *Science* 292(5524), 2011.

Burch T. E., Nagy K. L., and Lasaga A. C. (1993) Free energy dependence of albite dissolution kinetics at 80° C and pH 8.8. *Chemical Geology* 105(1-3), 137-162.

Cama J. G. J., Ayora C., and Lasaga C. A. (2000) Smetite dissolution kineitcs at 80 ° C and pH 8.8. *Geochimica et Cosmochimica Acta* 64(15), 2701-2717.

Carey J. W., Lichtner P. C., Rosen E. P., Ziock H. J., and Guthrie G. D. J. (2003) Geochemical mechanisms of serpentine and olivine carbonation. *Second annual conference on carbon sequestration*.

Crowley T. J. (2000) Causes of climate change over the past 1000 years. *Science* 289(5477), 270-277.

DOE. (1999) Carbon Sequestration Research and Development. U.S. Department of Energy.

Drever J. I. and Clow D. W. (1995) Weathering rates in catchments. In *Chemical Weathering Rates of Silicate Minerals*, Vol. 31 (ed. S. L. Brantley), pp. 463-481. Mineralogical Society of America.

Gunter W. D., Perkins E. H., and Hutcheon I. (2000) Aquifer disposal of acid gases: modelling of water-rock reactions for trapping of acid wastes. *Applied Geochemistry* 15(8), 1085-1095.

Gunter W. D., Wiwchar B., and Perkins E. H. (1997) Aquifer disposal of CO_2-rich greenhouse gases: extension of the time scale of experiment for CO2-sequestering reactions by geochemical modeling. *Mineralogy and Petrology* 59, 121-140.

Hammerstad T. (2000) Carbon dioxide storage prized. www.statoil.com.

Helgeson H. C. (1968) Evalution of irreversible reactions in geochemical processes involving minerals and aqueous solutions-1. Thermodynamic relations. *Geochimica et Cosmochimica Acta* 32, 853-877.

Helgeson H. C. (1979) Mass transfer among minerals and hydrothermal solutions. In *Geochemistry of Hydrothermal Ore Deposits* (ed. H. L. Barnes), pp. 568-610. John Wiley & Sons.

Helgeson H. C., Garrels R. M., and Mackenzie F. T. (1969) Evalution of irreversible reactions in geochemical processing involving minerals and aqueous solutions- II. Applications. *Geochimica et Cosmochimica Acta* 33, 455-481.

Helgeson H. C. and Murphy W. M. (1983) Calculation of mass transfer among minerals and aqueous solutions as a function of time and surface area in geochemical processes. I. computational approach. *Mathematical Geology* 15(1), 109-130.

Herzog H., Drake E., and Adams E. (1997) Reuse, and Storage Technologies for Mitigating Global Climate Change.

Hovorka S. D., Knox P. R., Holtz M. H., YEH J. S., Fouad K., and Sakurai S. (2002) Sequestration pilot site in the texas gulf cosast, USA. *GSA annual meeting & exposition abstracts with programs*, 135-10.

Johnson J. W., Nitao J. J., Steefel C. I., and Knauss K. G. (2002) Reactive transport modeling of geologic CO_2 sequestration. *GSA annual meeting & exposition abstracts with programs*, 174-1.

Johnson J. W., Oelkers E. H., and Helgeson H. C. (1992) SUPCRT92 - A software package for calculating the standard molal thermodynamic properties of minerals, gases, aqueous species, and reactions from 1-bar to 5000-bar and 0°C to 1000°C. *Computers and Geosciences* 18(7), 899-947.

Knauss K. G., Steefel C. I., Johnson J. W., and Boram L. H. (2002) Impact of CO_2, contaminant gas, aquesous fluid, and reservoir rock interactions o nthe geologic sequestration of CO_2. *GSA annual meeting & exposition abstracts with programs*, 135-13.

Lasaga A. C. (1998) *Kinetic Theory in the Earth Sciences*. Princeton University Press.

Nagy K. L. (1995) Dissolution and precipitation kinetics of sheet silicates. In *Chemical Weathering Rates of Silicate Minerals*, Vol. 31 (ed. A. F. W. a. S. L. Brantley), pp. 173-225. Mineralogical Society of America.

Nagy K. L. and Lasaga A. C. (1992) Dissolution and precipitation kinetics of gibbsite at 80° C and pH-3 - the dependence on solution saturation state. *Geochimica et Cosmochimica Acta* 56(8), 3093-3111.

NRC. (2003) Novel approaches to carbon management separation, capture, sequestration, and conversion to useful products workshop report. National Research council.

Oelkers E. H., Schott, J. and Devidal, J. L. . (1994) The effect of aluminum, pH, and chemical affinity on the rates of aluminosilicate dissolution reaction. *Geochim. Cosmochim. Acta,* 58, 2011-2024.

Palandri J. and Kharaka Y. (2003) Ferric iron minerals as geologic traps for CO_2 sequestration: iron reduction using sulfur-bearing waste gas. *Chemical Geology*, In review.

Parkhurst D. L., and Appello, A. A. J. . (1999) User's guide to PHREEQC (version 2)-a computer program for speciation, batch-reaction, one dimensional transport, and inverse geochemical modeling., pp. pp. 99-4259. U.S. Geological Survey.

Perkins E. H., Gunter W. D., Hutcheon I., Shevalier M., Durocher K., and Emberley S. (2002) Geochemical modelling and monitoring of CO_2 storage at the weyburn site, Saskatchewan, Canada. *GSA annual meeting & exposition abstracts with programs*, 174-11.

Seyfried W. E., Jr., Janecky D. R., and Berndt M. E. (1987) Rocking autoclaves for hydrothermal experiments; II, The flexible reaction-cell system. In *Hydrothermal Experimental Techniques* (ed. H. L. e. Barnes), pp. 216-239. Wiley-Intescience.

Shock E. L. and Helgeson H. C. (1988) Calculation of the thermodynamic and transport properties of aqueous species at high pressures and temperatures: Correlation algorithms for ionic species and equation of state predictions to 5 kb and 1000° C. *Geochimica et Cosmochimica Acta* 52, 2009-2036.

Shock E. L., Helgeson H. C., and Sverjensky D. A. (1989) Calculations of the thermodynamic and transport properties of aqueous species at high pressures and temperatures: Standard partial molal properties of inorganic neutral species. *Geochimica et Cosmochimica Acta* 53, 2157-2183.

Shock E. L., Oelkers E. H., Sverjensky D. A., Johnson J. W., and Helgeson H. C. (1992) Calculation of thermodynamic and transport properties of aqueous species at high pressures and temperatures. Effective electrostatic radii, dissociation constants and

standard partial molal properties to 1000°C and 5 kb. *J. Chem. Soc. London, Faraday Transactions* 88, 803-826.

Steefel C. I., and Van, Capppellen P. (1990) A new approach to modeling water-rock interaction: The role of precursors, nucleation, and Ostwald ripening. *Geochimica et Cosmochimica Acta* 54, 2657-2677.

Strazisar B. R., Tan H., Zhu C., and Hedges S. W. (2003) A reactive transport model of geochemical consequence upon injection of CO_2 into deep geological formations. *Journal of Contaminant Hydrology*, in review.

Sverjensky D. A., Shock E. L., and Helgeson H. C. (1997) Prediction of the thermodynamic properties of aqueous metal complexes to 1000 degrees C and 5 kb. *Geochimica et Cosmochimica Acta* 61(7), 1359-1412.

Truesdell A. H., Jones, B. F. (1974) Wateq, A computer program for calculating chemical equilibria of natural waters. *J. Res. U.S. Geol. Surv.* 2(2), 233-248.

White A. F. (1995) Chemical weathering of silicate minerals in soils. In *Chemical Weathering Rates of Silicate Minerals*, Vol. 31 (ed. S. L. Brantley), pp. 407-458. Mineralogical Society of America.

Xu T., Apps J. A., and Pruess K. (2003) Numerical simulation to study mineral trapping for CO_2 disposal in deep aquifers. *Applied Geochemistry*, (in press).

Zhu C., Blum A., and Veblen D. (2003) In situ feldspar dissolution rates in saturated aquifers. *Nature*, In review.